Journal of Alloys and Compounds 615 (2014) 719–727

Contents lists available at ScienceDirect

Journal of Alloys and Compounds

journal homepage: www.elsevier.com/locate/jalcom

X-ray analysis and optical studies of Dy^{3+} doped $NaSrB_5O_9$ microstructures for white light generation

G.R. Dillip [a], B. Ramesh [b], C. Madhukar Reddy [b], K. Mallikarjuna [b], O. Ravi [b], S.J. Dhoble [c], S.W. Joo [a], B. Deva Prasad Raju [d,*]

[a] School of Mechanical Engineering and Technology, Yeungnam University, Gyeongsan 712-749, South Korea
[b] Department of Physics, Sri Venkateswara University, Tirupati 517 502, India
[c] Department of Physics, RTM Nagpur University, Nagpur 440 033, India
[d] Department of Future Studies, Sri Venkateswara University, Tirupati 517 502, India

ARTICLE INFO

Article history:
Received 18 April 2014
Received in revised form 1 July 2014
Accepted 2 July 2014
Available online 10 July 2014

Keywords:
Phosphor
Strain analysis
Microstructure
Luminescence

ABSTRACT

A white light emitting phosphor $NaSrB_5O_9:Dy^{3+}$ was synthesized by a conventional solid state reaction method. The structure of the phosphors was analyzed by powder X-ray diffraction (XRD), revealing that the phosphors crystallized in monoclinic crystal structure with the space group ($P2_1/c$). Williamson–Hall (W–H) analysis was used to study the individual contributions of crystallite sizes and lattice strain on the peak broadening of $NaSrB_5O_9:Dy^{3+}$ phosphors. Monoclinic microstructures of nearly plate-like morphologies were observed in the FE-SEM images. Upon near-UV excitation wavelength (390 nm), the blue emission at ~482 nm ($^6H_{15/2}$) and yellow emission at ~584 nm ($^6H_{13/2}$) were observed in the phosphors. The critical quenching concentration of Dy^{3+} in $NaSrB_5O_9$ phosphor was found to be 3 at.% with the critical distance (R_c) of ~22.30 Å and the corresponding concentration quenching mechanism was testified to be the exchange interaction between the dopant Dy^{3+} ions. In order to investigate the application in white LEDs, the Commission International de l'Eclairage (CIE) chromaticity coordinates, color temperature and decay curve measurements of Dy^{3+} ions doped $NaSrB_5O_9$ phosphors were carried out. The yellow to blue (Y/B) emission integrated intensity ratio is maximum (~0.9) for all the concentrations, suggesting that the phosphors favor for white illumination.

1. Introduction

In recent years, rare earth (RE) ions doped luminescence materials have been widely studied and applied for a wide variety of applications due to their unique physical and chemical properties. It includes the optical transmission, television tubes, mobile telephone screens, biochemical probes, medical diagnosis and promising white light emitting diodes [1–3]. Due to the superior characteristics over traditional light emitting diodes (i.e. the blue light emitting diodes), the phosphor converted white light emitting diodes (*w*-LEDs) have made a significant revolution in the field of illumination. *w*-LEDs are excellent candidates for general lighting applications and have attracted interesting attention due to the advantages of rapidly improving efficiency, durability, reliability, long lifetime, high luminescence efficiency and environmental friendliness [4,5]. Effective lighting devices can be realized by combining one or more phosphors with chips. Currently, the conventional phosphor-converted *w*-LEDs have been produced by a combination of blue LED coated with yellow phosphor or UV excited tricolor, red, green and blue (RGB) phosphors. UV phosphor converted LEDs are expected to have many potential applications due to their excellent optical stability, high color tolerance and high conversion efficiency. However, the problems with these traditional white LEDs are high thermal quenching and poor color rendering index (RI), and suitable color correlated temperature (CCT) that can generate warm/cool/day white light. These problems can be overcome by using a single-phase phosphor, effectively excited in near-UV (NUV) range that emits simultaneously red, green and blue light whose combination produces white light [6–8]. Recently, Zhang and Gong studied and reported a single-phased white light emitting $NaCaBO_3:Ce^{3+}$, Tb^{3+}, Mn^{2+} phosphor for LED applications [9]. Alternatively, Aboulaich et al., fabricated the warm white light emitting diodes using the combination of Ce-doped YAG nanophosphors and red emitting semiconductor quantum dots [10]. Although some thousands of phosphors have been synthesized and characterized in the past several years, the range of phosphors that are suitable for *w*-LEDs is limited. The progress has to be made in the

* Corresponding author. Tel.: +91 94402 81769.
E-mail address: drdevaprasadraju@gmail.com (B.D.P. Raju).

http://dx.doi.org/10.1016/j.jallcom.2014.07.017
0925-8388/

preparation and development of such phosphors. Hence, the careful selection of phosphors that is efficiently excited by near UV light is highly desirable and suggests an opportunity for further development. Several scientific challenges, however, must be overcome before the selected phosphors can be practically applied in LEDs.

Over the past, the phosphors based on borate host matrices have been investigated due to the advantages such as low synthetic temperature, high stability, low cost and high luminescence efficiency over other materials. Borate materials doped with Dy^{3+} ions have attracted for its white light emission [11,12]. Various researchers are trying to explore the luminescence properties of Dy^{3+} ions in different compositions. The Dy^{3+} ion has two intense fluorescence transitions in the blue and yellow regions, which makes the Dy^{3+} ions doped phosphors to be good candidate for solid state lighting devices. Thus, white light can be obtained from Dy^{3+} activated materials by either changing the intensity ratio of the blue to yellow emissions or by adjusting the host composition [13,14].

Over the past few years, our group has been devoted to investigate the various suitable phosphors for white light emitting diodes. In this scenario, some of the phosphors studied were reported in the literature on RE^{3+} ions doped phosphate and borate host matrices. For instance, $Ba_3Ca_3(PO_4)_4:Eu^{3+}$ [15], $NaSrB_5O_9:Eu^{3+}$ [16] and $Na_3SrB_5O_{10}:Dy^{3+}$ [17], etc. In 2007, Wu et al., first synthesized the new pentaborate $NaSrB_5O_9$ and reported the crystal structure and its chemical composition [18]. In the present investigation, we have synthesized and studied systematically the novel $NaSrB_5O_9$ phosphors doped with Dy^{3+} ions. To the best of our knowledge, no reports have appeared in the literature on the luminescence properties of $NaSrB_5O_9:Dy^{3+}$ microstructures. In this communication, an attempt has been made by the authors to explore the relation between the crystal structure by employing W–H analysis and luminescence properties of the proposed microstructures. The obtained results suggest that this new $NaSrB_5O_9:Dy^{3+}$ phosphors might be useful for near UV converted *w*-LEDs.

2. Experimental methods

In a typical experiment, the undoped and Dy^{3+} ions doped $NaSrB_5O_9$ phosphors were prepared using high temperature solid state reaction method by sintering the samples at 800 °C in air atmosphere. The analytical reagent (AR) grade raw materials used for powder synthesis are Na_2CO_3 (99.99%), $SrCO_3$ (99.99%), H_3BO_3 (99.9%), and Dy_2O_3 (99.9%) and all were used as received, without further purification. The dopant concentration was varied from 1, 2, 3, 5 and 7 at.% in the host matrix. The stoichiometric ratios of these samples were first mixed homogeneously by an agate mortar for 1 h. Then, the mixture was kept in a porcelain crucible and sintered at 800 °C in an electric furnace and kept at this temperature for 8 h. After sintering, the samples were cooled to room temperature (RT) in the furnace, and finally, ground again into powder for further measurements.

The structure of the phosphors was analyzed on a PANalytical X'Pert PRO X-ray diffractometer with Cu Kα radiation (λ = 0.154056 nm) at 40 kV and 30 mA and a PIXcell solid state detector was used. The data was collected over a 2θ range from 10° to 80° in the step scan mode with a step size of 0.02°. Fourier transform infrared (FTIR) spectra were recorded on a Bruker Alpha-T FT-IR spectrophotometer using KBr pellets in the spectral range of 4000–500 cm^{-1}. The surface morphology and microstructure of the samples were examined using a field emission scanning electron microscope (FE-SEM, Hitachi S-4200, Japan). The presence of dopant element (Dy) in the prepared samples was confirmed by energy dispersive X-ray analysis (EDS) on the FE-SEM attached EDS instrument. To conduct the powders, a thin layer of platinum is coated on the sample surface. UV–Vis diffuse reflectance spectra (DRS) of phosphors were recorded on UV–Vis spectrophotometer (Jobin Varian Cary 5000) using a polytetrafluoroethylene (PTFE) as a reference sample. The excitation, fluorescence and decay measurements were carried out using Jobin Yvon Fluorolog-3 fluorimeter with a xenon lamp as the excitation source. All the measurements were carried out at RT.

3. Results and discussion

3.1. XRD analysis

The crystallinity and phase purity of $NaSrB_5O_9:Dy^{3+}$ phosphors were examined by powder XRD measurements. Fig. 1 shows the comparison of XRD patterns of the prepared samples over the standard XRD data, Joint Committee on Powder Diffraction Standards (JCPDS). All the noticeable peaks for all samples were indexed as the $NaSrB_5O_9$ borate crystal of monoclinic crystal structure found in the JCPDS Card No: 056-0415. It was identified that no Dy_2O_3 peaks were present in the patterns. However, due to the increase of dopant concentration the predominant diffraction peaks are also shifted towards the higher 2θ angle side, suggesting that the introduced Dy^{3+} ions are incorporated in the host cation sites. Due to the disparity of ionic sizes and different valance states among B^{3+} (0.11 Å, CN = 4)/Dy^{3+} (1.03 Å, CN = 8)/Sr^{2+} (1.26 Å, CN = 8)/Na^{+}(0.39 Å, CN = 6), the authors considered that the possible sites for incorporating the Dy^{3+} ions are at Sr^{2+} cation sites in $NaSrB_5O_9$ host. The possible reason for the shifting of XRD peaks are that the Dy^{3+} ions has a smaller ionic radius (1.03 Å, CN = 8) than that of cation, Sr^{2+} (1.26 Å, CN = 8) [17,19,20]. The dopant, Dy^{3+} ions substitution in the host cation sites cause the lattice contraction, producing an internal stress and shifting the XRD peaks to the higher angle side. To give evidence of the lattice contraction, the monoclinic crystal structure parameters such as lattice constants *a*, *b* and *c* and unit cell volume are estimated from the lattice geometry equations using the following relations,

$$\frac{1}{d^2} = \frac{1}{\sin^2\beta}\left(\frac{h^2}{a^2} + \frac{k^2\sin^2\beta}{b^2} + \frac{l^2}{c^2} + \frac{2hl\cos\beta}{ac}\right) \quad (1)$$

$$\text{and} \quad V = abc\sin\beta \quad (2)$$

where *d* is the distance between adjacent planes (nm), (*hkl*), the miller indices, *a*, *b*, *c* and β, the lattice constants (nm) and *V* is the unit cell volume (nm^3). Here, the authors considered the dominant intensity lattice planes of (0 2 0), (0 1 2) and (2 3 0) at around 12.66°, 29.42° and 30.10° for interplanar distances d_1, d_2 and d_3, respectively and β = 106.907° (*JCPDS data*) to calculate the unit cell parameters. The estimated lattice parameters of the microstructures are summarized in Table 1. It is noticed from the table that the volume is decreased owing to the increase of Dy^{3+} ions concentration, suggesting the lattice shrinkage with the results of internal tensile stress generated in the crystal.

3.1.1. Crystallite size and strain analysis

To further justify the lattice contraction, the size and strain analysis of the synthesized phosphors were performed using the XRD data with the Williamson–Hall method. In the W–H method, the observed breadth results from the sum of Scherrer's equation (particles size) and strain, $\varepsilon \approx \frac{\beta_s}{\tan\theta}$ and is given by the following equation [21,22];

$$\beta = \beta_s + \beta_D = \left(\frac{k\lambda}{D\cos\theta}\right) + (4\varepsilon\tan\theta) \quad (3)$$

$$\text{Finally we get,} \quad \beta\cos\theta = \left(\frac{k\lambda}{D}\right) + (4\varepsilon\sin\theta) \quad (4)$$

where *D* is the crystallite size in nanometers, λ, the wavelength of X-rays (0.154056 nm for Cu Kα radiation), *k* is the shape factor, θ, the peak position (°) and β is the full width at half maximum (FWHM) intensity (radians). Here, the authors suppressed the instrumental broadening to estimate the size and strain of the phosphors, because the instrumental broadening effect may shift the size-strain plot along the vertical axis without changing the slope to a significant extent. Hence, it might be induce some errors in the estimation of size, but will not affect the strain values significantly. Therefore, the plots were drawn with 4 sinθ on *x*-axis and βcosθ along the *y*-axis for all phosphors giving the straight lines, shown in Fig. 2. By fitting the data to the equation, $y = mx + c$ with 5% error estimation, the strain (ε) was extracted from slope of the

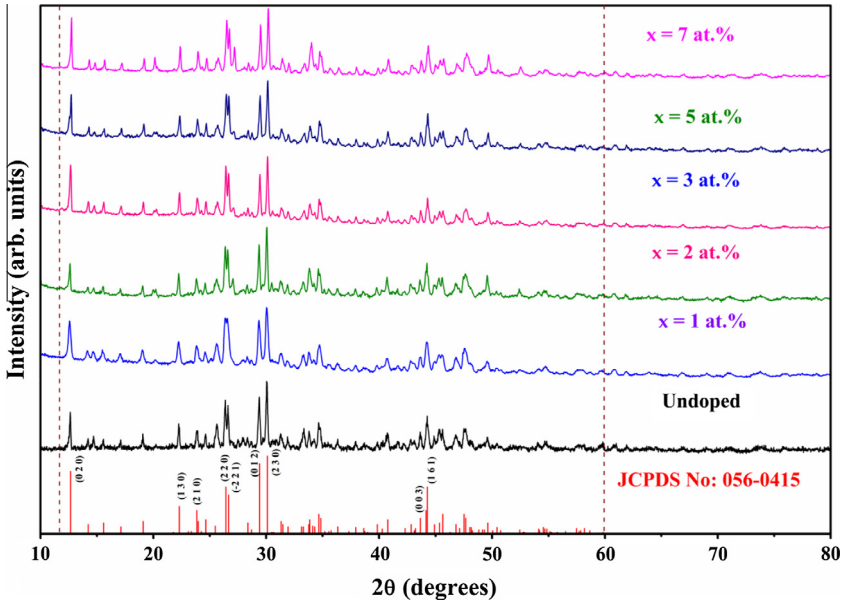

Fig. 1. XRD patterns of $NaSr_{1-x}B_5O_9:Dy_x^{3+}$ (x = 0–7 at.%) phosphors.

Table 1
Structural parameters, crystallite size (D), microstrain (ε), X-ray density (ρ), Y/B ratio, lifetimes and CCT values of $NaSrB_5O_9:Dy^{3+}$ phosphors.

Samples	d-Spacing along *hkl* planes (∼nm)			Lattice parameters				D (∼nm) (W–H plots)	Strain (∼10^{-4})		ρ (∼gm/cm^3)	Y/B ratio	Lifetimes (∼μs)	CCT values (∼K)
	(020)	(012)	(230)	a (∼nm)	B (∼nm)	c (∼nm)	Volume (∼nm^3)		W–H plots	$\varepsilon_{(230)}$				
Undoped	0.69995	0.30397	0.29724	0.80601	1.39990	0.65093	0.70272	59 ± 2.9	6.19 ± 0.31	6.36	2.917	–	–	–
1 at.%	0.70167	0.30335	0.29716	0.80430	1.40334	0.64939	0.70130	34 ± 1.7	9.82 ± 0.49	9.35	2.930	0.908	931	8095
2 at.%	0.70223	0.30332	0.29706	0.80342	1.40446	0.64936	0.70106	54 ± 2.7	5.32 ± 0.26	5.16	2.945	0.983	920	6365
3 at.%	0.69962	0.30310	0.29645	0.80267	1.39924	0.64899	0.69740	61 ± 3.1	7.81 ± 0.39	7.46	2.963	0.971	867	7848
5 at.%	0.69677	0.30284	0.29622	0.80386	1.39354	0.64854	0.69510	47 ± 2.4	6.94 ± 0.34	6.71	2.975	0.969	859	8059
7 at.%	0.69478	0.30257	0.29571	0.80310	1.38956	0.64802	0.69191	71 ± 3.6	5.13 ± 0.25	5.27	3.013	0.976	–	6066
JCPDS	0.69858	0.30333	0.29658	0.80427	1.39706	0.64956	0.69831	–	–	–	–	–	–	–

line; the y-intercept ($\frac{\lambda}{D}$) gives the crystallite size (D). The results are summarized in Table 1. The '−ve' values of strain from the slope of lines suggest that this may be due to the lattice shrinkage in the crystal, which was also consistent with the calculated unit cell volume from the crystal geometrical equations (Table 1). From the table, it is noticed that the various crystallite sizes may be due to the non-uniform strain generated in the crystal. In addition, the density (ρ) and micro strain (ε) were estimated using the following relations [23],

$$\rho = \frac{ZM}{N_A V} \tag{5}$$

$$\text{and } \varepsilon = \frac{\beta \cos\theta}{4} \tag{6}$$

where M is the molecular mass (grams/mol), Z is the formula units per cell, N_A is Avogadro's number (6.0221×10^{-23} particles/mol), V is the unit cell volume (nm)^3 and ρ is in gram/cm^3. The estimated values are presented in Table 1. It is observed from the table that the density values are steadily increased with the raise of dopant concentration.

3.2. FTIR studies

The FTIR spectra were measured to substantiate the coordination surrounding the B–O in $NaSrB_5O_9:Dy^{3+}$ samples and is shown in Fig. 3. From the spectra, it is clear that the strong absorption band at ∼561 cm^{-1} may be due to Na–O and Sr–O vibrations. In the region between 703 and 826 cm^{-1}, the bands associated with BO_3 and BO_4 out of plane bending modes are overlapped [24]. The bands near ∼971 and ∼1002 cm^{-1} mainly attributed to tetrahedrally coordinated boron group (BO_4) asymmetric stretching vibrations, while the strong band at about 1313 cm^{-1} for all samples should be ascribed to the stretching modes of trigonally coordinated boron (BO_3) groups. The broad absorption band located at around 3491 cm^{-1} is due to the presence of —OH group in the samples. It is the characteristic vibrations of water from air, which might be physically absorbed water on the sample surface during the grinding process [17].

3.3. FE-SEM and EDS analysis

The surface morphological features of the Dy^{3+} ions doped $NaSrB_5O_9$ samples are shown in Fig. 4. Generally, in the solid state reaction method, the morphology of phosphors mainly depends on the uniformity of grinding, homogeneity of the sample and the morphology of precursors used. From the figure, it is clearly noticed that there is no appreciable changes in the morphology of phosphors due to the increase of Dy^{3+} ions concentration, the agglomerations of the particles are also poor. The phosphor is formed by the irregular grains; some of them appear to have a nearly plate-like morphology in the micrometer dimension. A

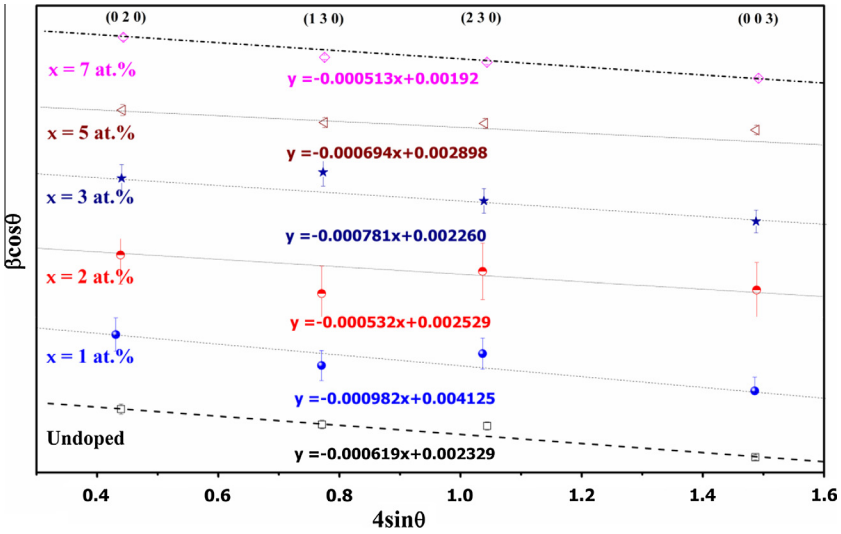

Fig. 2. The W–H analysis of $NaSr_{1-x}B_5O_9:Dy_x^{3+}$ (x = 0–7 at.%) phosphors.

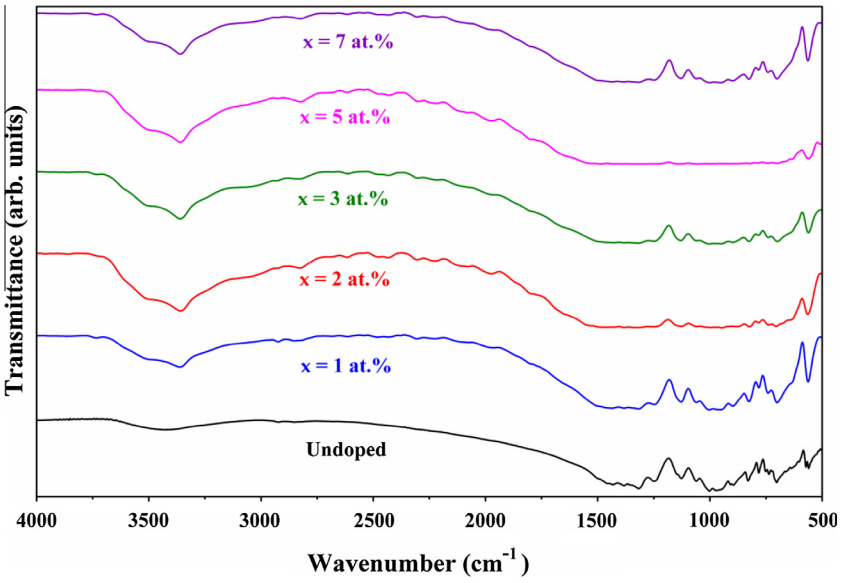

Fig. 3. FTIR spectra of $NaSr_{1-x}B_5O_9:Dy_x^{3+}$ (x = 0–7 at.%) phosphors.

detailed examination of the SEM micrograph of 3 at.% Dy^{3+} doped phosphor indicated that the number of non-uniform dimension plates are arranged in vertical direction to form the microstructure of the phosphor. Interestingly, more precise observations of the images suggest that the morphology of some of the plate seems to be like a monoclinic crystal structure of the phosphors (*highlighted on the images* (Fig. 4) *by white circles*), which is highly correlated with XRD results. Thus, this type of different morphology with micrometer dimension will find more applications such as solid state lighting devices. The EDS analysis was carried out for qualitative elemental analysis of the dysprosium ion in the $NaSrB_5O_9:Dy^{3+}$ phosphors. The EDS profiles are shown in Fig. 5 and confirmed the presence of the dopant (Dy) in the $NaSrB_5O_9:Dy^{3+}$ phosphors. The approximate estimation of elemental percentage of Na, Sr, O and Dy is shown in the inset of Fig. 5(c) for 3 at.% Dy^{3+} doped $NaSrB_5O_9$ phosphor as a reference. Thus, the absence of other impurity elements in EDS profiles is an evidence of the phase purity of the obtained phosphor and consistent with the structural analysis.

3.4. DRS measurements

Fig 6 shows the recorded DRS of $NaSrB_5O_9:Dy^{3+}$ (Dy^{3+} = 0–7 at.%) phosphors. It is observed from the spectra that the strong absorption band at ~240 nm is due to boron to oxygen (B–O) charge transition (CT) in host matrix and this band is shifted towards the lower wavelength region (i.e. higher energy side) due to the increase of Dy^{3+} ions concentration, which is consistent with XRD results [25]. In the range from 300 to 800 nm, the host material shows a platform of high reflectance, while the bands observed at around 326 ($^6H_{15/2} \rightarrow {}^4L_{19/2}$), 352 ($^6H_{15/2} \rightarrow {}^4I_{11/2}$), 365 ($^6H_{15/2} \rightarrow {}^6P_{7/2}$) and 386 nm ($^6H_{15/2} \rightarrow {}^4I_{13/2}$) correspond to f–f transition of Dy^{3+} ions in $NaSrB_5O_9:Dy^{3+}$ phosphors [17]. These absorption bands become stronger with the increase of dopant concentration. In the region between 300 and 400 nm (inset of Fig. 6), the major absorption bands observed in DRS is consistent with those obtained from the excitation spectra. Hence, it is clear from the DRS that due to the introduction of Dy^{3+} ions in the host enhance the optical absorption in the near UV region.

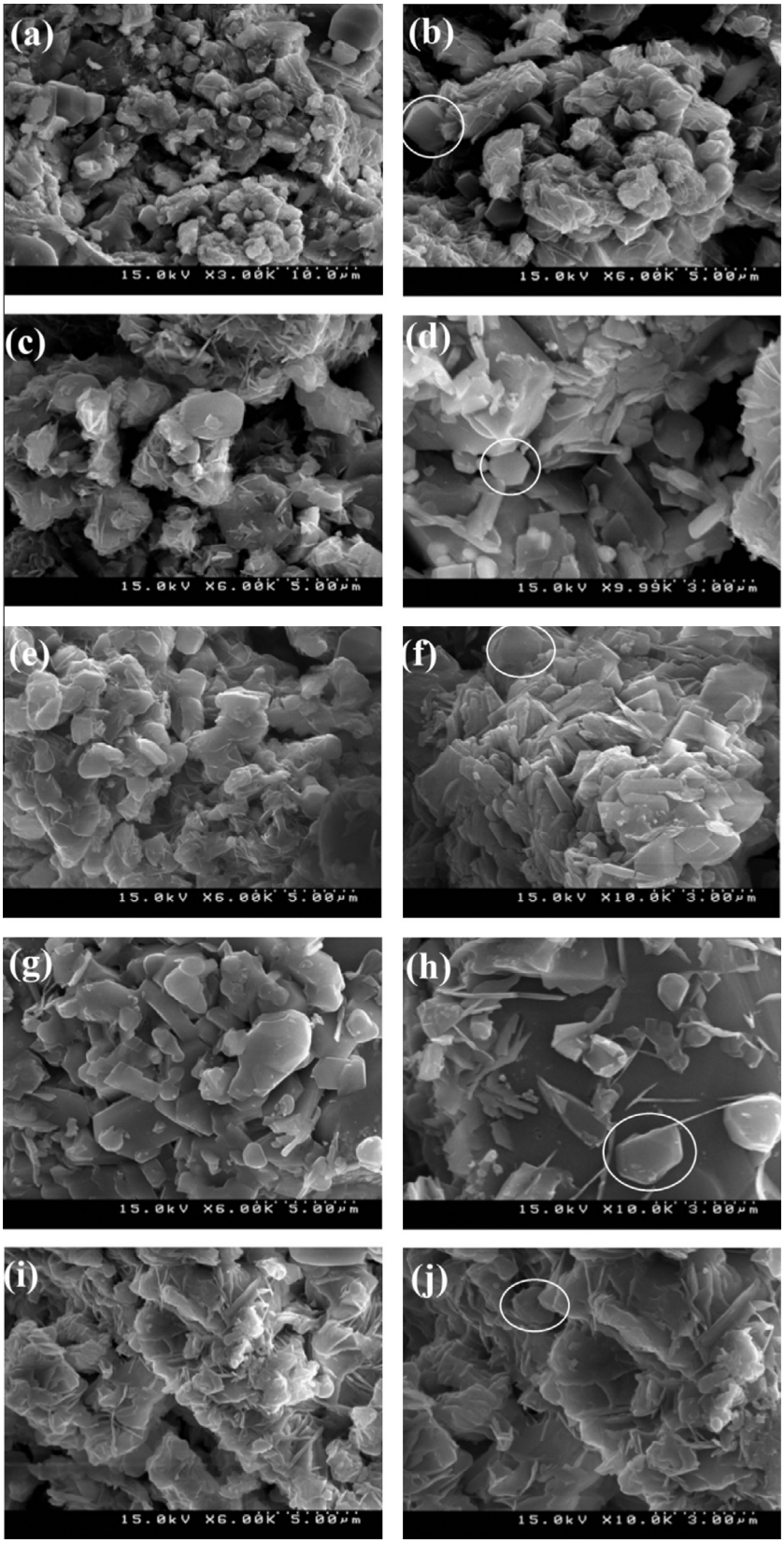

Fig. 4. FE-SEM images of $NaSr_{1-x}B_5O_9:Dy_x^{3+}$ (x = 1–7 at.%) phosphors, (a and b) x = 1 at.%, (c and d) x = 2 at.%, (e and f) x = 3 at.%, (g and h) x = 5 at.% and (i and j) x = 7 at.%.

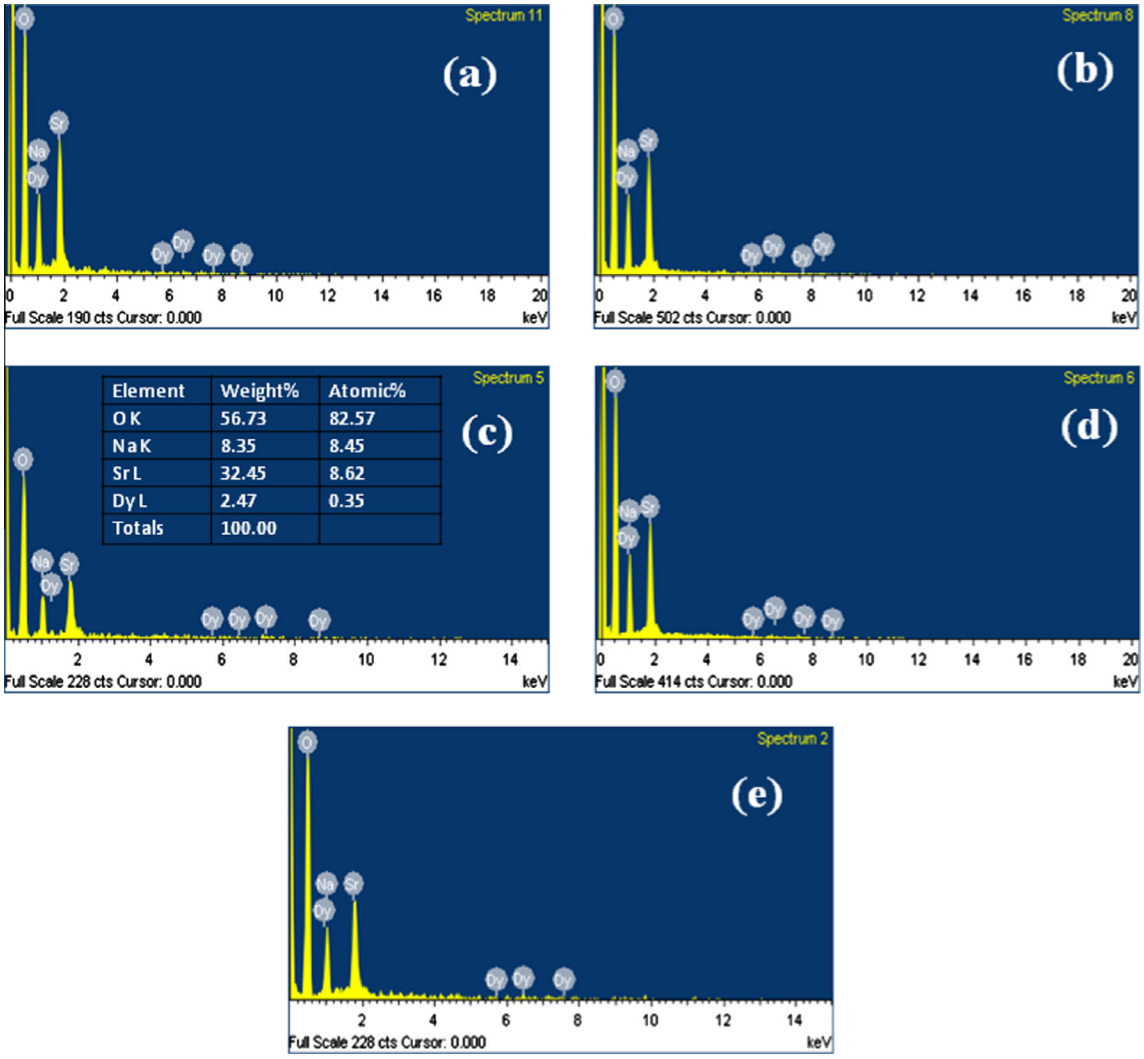

Fig. 5. EDS profiles of $NaSr_{1-x}B_5O_9:Dy_x^{3+}$ ($x = a - e = 1–7$ at.%) phosphors.

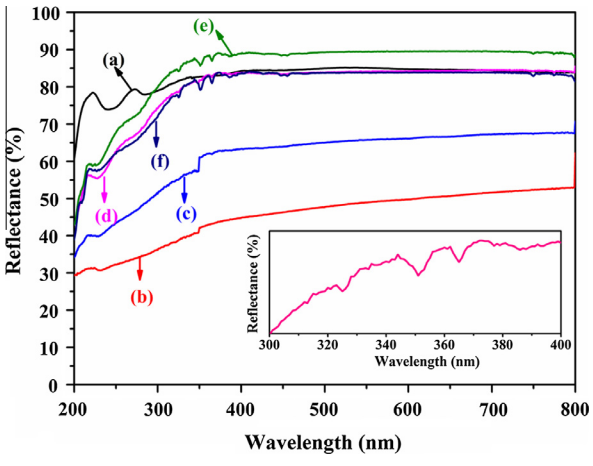

Fig. 6. UV–Vis DRS of $NaSr_{1-x}B_5O_9:Dy_x^{3+}$ ($x = a - f = 0–7$ at.%) phosphors. Inset shows the expansion of DRS ($Dy^{3+} = 3$ at.%) between 300 and 400 nm.

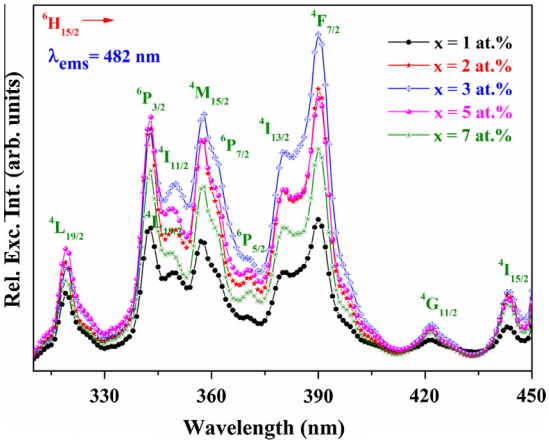

Fig. 7. Excitation spectra of $NaSr_{1-x}B_5O_9:Dy_x^{3+}$ ($x = 1–7$ at.%) phosphors.

3.5. Excitation and emission spectra

The excitation spectra of $NaSrB_5O_9:Dy^{3+}$ ($Dy^{3+} = 1–7$ at.%) phosphors at 482 nm emission wavelength is shown in Fig. 7. The spectra consists of several peaks correspond to $^6H_{15/2} \rightarrow {}^4L_{19/2}$, $^6P_{3/2}$, $^4I_{11/2}$, $^4M_{15/2}$, $^6P_{7/2}$, $^6P_{5/2}$, $^4I_{13/2}$, $^4F_{7/2}$, $^4G_{11/2}$ and $^4I_{15/2}$ excited from $^6H_{15/2}$ ground state to various levels located at about 319, 343, 350, 358, 362, 370, 380, 390, 421 and 443 nm, respectively [26,27]. Among the several sharp lines, the dominant intense excitation peak at 390 nm corresponds to $^6H_{15/2} \rightarrow {}^4F_{7/2}$ transition is

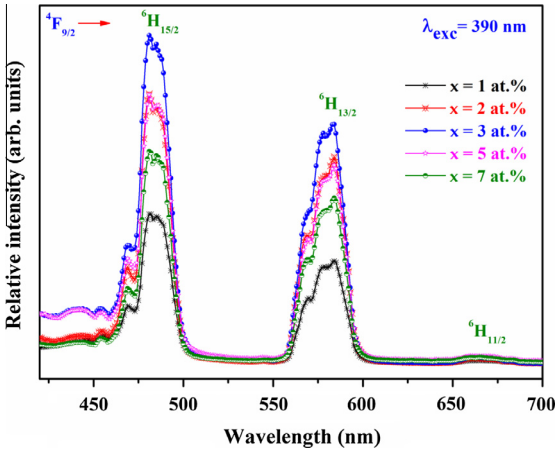

Fig. 8. Emission spectra of $NaSr_{1-x}B_5O_9:Dy_x^{3+}$ (x = 1–7 at.%) phosphors.

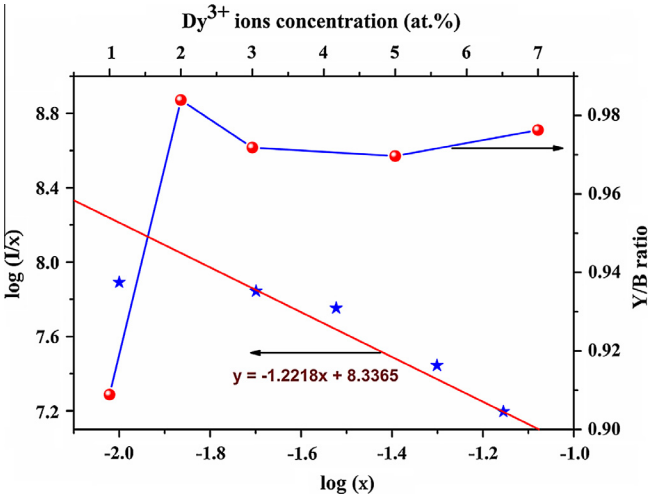

Fig. 9. Plot of log(I/x) versus log(x) (left) and the variation of Y/B ratio with Dy^{3+} ions (right).

used to study the emission spectra for all samples. The most intense peak obtained at 390 nm clearly suggests that these phosphors are effectively excited by near UV white light emitting diodes.

The emission spectra of $NaSrB_5O_9:Dy^{3+}$ (Dy^{3+} = 1–7 at.%) phosphors, excited at 390 nm are shown in Fig. 8. The emission spectra have similar shapes for all Dy^{3+} doped samples and no peak shifting was observed. They consists of two predominant emission bands at around 482 nm (blue) and the other at ~584 nm (yellow) corresponding to $^4F_{9/2} \rightarrow {}^6H_{15/2}$ and $^4F_{9/2} \rightarrow {}^6H_{13/2}$ transitions, respectively; the other weak emission peak at ~665 nm corresponds to $^4F_{9/2} \rightarrow {}^6H_{11/2}$. The magnetic dipole (*MD*) $^4F_{9/2} \rightarrow {}^6H_{15/2}$ transition varies with the crystal field strength around Dy^{3+} ions, is more intense than the electric dipole (*ED*) $^4F_{9/2} \rightarrow {}^6H_{13/2}$ transition and belongs to a hypersensitive transition ($\Delta L = 2$ and $\Delta J = 2$), which is strongly influenced by the chemical environment surrounding the Dy^{3+} ions [28], suggesting that the Dy^{3+} ions occupy the symmetric site with high inversion symmetry. The site symmetry surrounding the Dy^{3+} ions can be confirmed by the yellow to blue integrated intensity ratio between the two transitions. A ratio greater than 1 indicates the symmetric environment of Dy^{3+} ion. In the present case, this ratio changes with concentration indicating the variation in symmetric nature of Dy^{3+} ion inside $NaSrB_5O_9$. The higher value of this ratio (>0.9) implies the high symmetric nature of Dy^{3+} ions in the $NaSrB_5O_9$ with an inversion center. To investigate the Dy^{3+} concentration effect on the emission intensity, the Dy^{3+} ion concentration was systematically varied in the $NaSrB_5O_9$ system. Effect of concentration of Dy^{3+} ion on Y/B emission intensity ratio of $NaSrB_5O_9$ phosphor is shown in Fig. 9. The calculated Y/B intensity ratios are presented in Table 1. From the emission spectra, it is observed that with the increase of Dy^{3+} ions concentration up to 3 at.%, the intensity of both the blue and yellow emissions steadily improves, but then rapidly deteriorates due to concentration quenching of Dy^{3+} emission. In many inorganic materials, an extreme doping of emission ions usually decreases the emission intensity surprisingly, due to the fact that strong interaction occurs between activating ions with reduced distance, resulting a concentration quenching [29]. The concentration quenching may occur because the excitation energy migrates about a large number of centers before being emitted. Due to the non-radiative energy transfer between luminescent centers (dopant ions), the emission intensity decreased after 3 at.% Dy^{3+} ions. Dexter developed a theoretical model on the relationship between emission intensity and activator concentration, according to which the multipolar interaction between the same type of activator (Dy^{3+}) ions in the solid phosphors can be concluded by analysing the constant θ according to the equation [30];

$$\frac{I}{x} = k[1 + \beta(x)^{\theta/d}]^{-1} \quad (7)$$

where I is the emission intensity, x is the activator content, d is the samples dimension (d = 3 for energy transfer among the activators inside particles), k and β are the constants (independent of activator concentration) and θ is the index of electric multipole. The index θ can be 6, 8 and 10 for the dipole–dipole, dipole-quadrupole and quadrupole–qaudrupole electric interactions, respectively; θ = 3 corresponds to exchange interactions. The plot of log(I/x) verses log(x) at 482 nm emission is shown in Fig. 9, which gives a linear fit having an y-intercept ~8.336 and a slope ($-\theta/3$) of −1.2218, yielding an θ value of ~3.66, which is nearly close to 3. Hence, the concentration dependent emission spectra indicates that the concentration quenching for the two Dy^{3+} ions was caused by exchange interaction in the $NaSrB_5O_9:Dy^{3+}$ phosphors [31]. The separation between the donors (activators) and acceptors (quenching site) can be known by critical distance (R_c) parameter, between the same activators by using the relation,

$$R_c = 2(3V/4\pi X_c N)^{1/3} \quad (8)$$

where V is the volume of the unit cell (Å^3), X_c is the critical concentration of the activator ion and N is the number of host cations (Sr^{2+}) in the unit cell [32]. In the present phosphor, the values of V, X_c and N are 697.47 Å^3, 0.03 and 4, respectively. The critical transfer distance of Dy^{3+} ions in $NaSrB_5O_9$ phosphors is found to be ~22.30 Å.

3.6. Decay curve analysis

In order to obtain additional information on the luminescence properties of Dy^{3+} ions in $NaSrB_5O_9$ phosphors, the decay curve measurements were employed. Fig. 10 shows the decay curves of $^4F_{9/2} \rightarrow {}^6H_{15/2}$ (482 nm) emission for these samples, excited at 390 nm. All the decay curves were well fitted by a second order exponential function applying the following equation;

$$I(t) = A_1 \exp(-t/\tau_1) + A_2 \exp(-t/\tau_2) \quad (9)$$

where A_1 and A_2 are the fitting parameters and τ_1 and τ_2 are the lifetimes. The average lifetimes could be calculated using the relation [33];

$$\tau = (A_1\tau_1^2 + A_2\tau_2^2)/(A_1\tau_1 + A_2\tau_2) \quad (10)$$

The estimated lifetimes are presented in Table 1. With the increase of Dy^{3+} ions concentration, the lifetimes decreased due to the fact that both the energy transfer rate between Dy^{3+} and

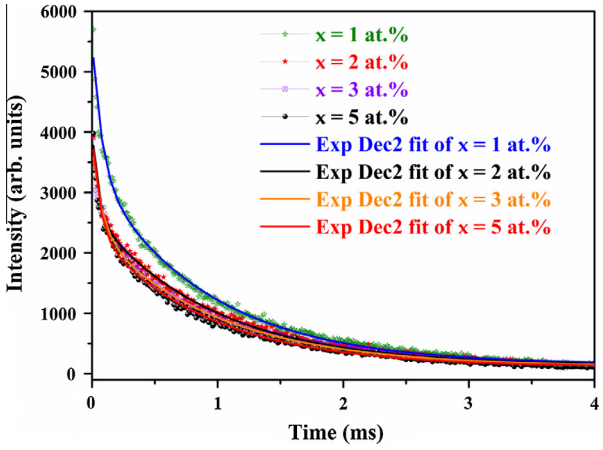

Fig. 10. Decay curves of $NaSr_{1-x}B_5O_9:Dy_x^{3+}$ (x = 1–5 at.%) phosphors.

Dy^{3+} and the probability of energy transfer to luminescent killer sites (such as defects) increased. However, the lifetime values obtained in the present investigations are comparable to those reported on the Dy^{3+} doped phosphors in literature [17,34,35].

3.7. CIE and CCT analysis

In order to examine the possible application of the $NaSrB_5O_9:Dy^{3+}$ phosphors in *w*-LEDs, the CIE 1931 chromaticity coordinates are calculated. The chromaticity coordinates for $NaSrB_5O_9:Dy^{3+}$ phosphors with different dopant contents are estimated from the emission spectra, excited by 390 nm. The obtained color coordinates all are located within the white light region of the CIE 1931 chromaticity diagram, shown in Fig. 11. To investigate the quality of white light, the CCT values are calculated using McCamy's empirical formula [36]:

$$CCT = -449n^3 + 3525n^2 - 6823.3n + 5520.33 \quad (11)$$

where $n = (x - x_e)/(y - y_e)$ is the inverse slope line and (x_e = 0.332, y_e = 0.186) is the epicenter. The estimated CCT values are listed in Table 1. Hence, the present phosphors might be applicable for the generation of cool/day white light emission excitable at UV (390 nm) LED in the field of solid state lighting.

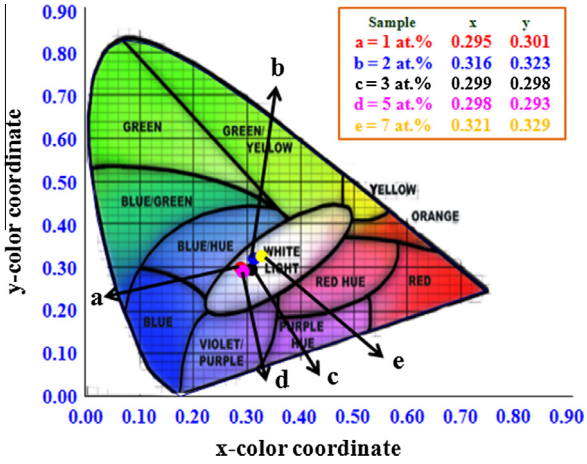

Fig. 11. CIE chromaticity coordinates of $NaSr_{1-x}B_5O_9:Dy_x^{3+}$ (x = 1–7 at.%) phosphors.

4. Conclusions

In conclusion, a series of $NaSrB_5O_9:Dy^{3+}$ microstructures were synthesized by single step solid state reaction method at 800 °C in air atmosphere. The XRD results revealed that the predominant diffraction peaks were shifted towards the higher energy side due to the substitution of Dy^{3+} ions at Sr^{2+} cation sites in $NaSrB_5O_9$ host material. The size and strain contributions to line broadening of $NaSrB_5O_9:Dy^{3+}$ powders were analyzed by Williamson and Hall analysis. Plate-like morphology in micrometer dimension is identified by SEM analysis and some of the plates present monoclinic crystal morphology. The characteristic emission bands of Dy^{3+} ions were observed at about 482 nm and 584 nm for all samples in the PL spectra. The optimized Dy^{3+} ions concentration was found to be 3 at.% with the critical distance of ~22.30 Å and also the corresponding concentration quenching mechanism was found to be the exchange interaction between the Dy^{3+} ions inside the crystal. Moreover, the CIE chromaticity coordinates located within the white light region and the calculated CCT values located in the cool/day white light region. Hence, the phosphors might be useful for the fabrication of SSL devices.

Acknowledgements

The corresponding author, B. Deva Prasad Raju is highly grateful to DST-SERB, Department of Science and Technology, Government of India, India, for providing financial assistance in the form of major research project; vide reference number, SERB SB EMEQ-037-2013; dated-17-12-2013.

References

[1] M. Que, Z. Ci, Y. Wang, G. Zhu, Y. Shi, S. Xin, J. Lumin. 144 (2013) 64–68.
[2] M. Shang, C. Li, J. Lin, Chem. Soc. Rev. 43 (2014) 1372–1386.
[3] C.C. Lin, R.S. Liu, J. Phys. Chem. Lett. 2 (2011) 1268–1277.
[4] T. Nishida, T. Ban, N. Kobayashi, Appl. Phys. Lett. 82 (2003) 3817–3819.
[5] A. Khanna, P.S. Dutta, J. Solid State Chem. 198 (2013) 93–100.
[6] E. Downing, L. Hesselink, J. Ralston, R.R. Macfarlane, Science 273 (1996) 1185–1189.
[7] S.K.K. Shaat, H.C. Swart, O.M. Ntwaeaborwa, Opt. Mater. Express 2 (2012) 962–968.
[8] Z.W. Zhang, A.J. Song, M.Z. Ma, X.Y. Zhang, Y. Yue, R.P. Liu, J. Alloys Comp. 601 (2014) 231–233.
[9] X. Zhang, M. Gong, Dalton Trans. 43 (2014) 2465–2472.
[10] A. Aboulaich, M. Michalska, R. Schneider, A. Potdevin, J. Deschamps, R. Deloncle, G. Chadeyron, R. Mahiou, ACS Appl. Mater. Inter. 6 (2014) 252–258.
[11] U. Fawad, M. Oh, H. Park, S. Kim, H.J. Kim, J. Alloys Comp. 610 (2014) 281–287.
[12] X. Zhang, Y. Chen, L. Zhou, M. Gong, Mater. Lett. 93 (2013) 390–392.
[13] Q. Su, Z. Pei, L. Chi, H. Zhang, Z. Zhang, F. Zou, J. Alloys Comp. 192 (1993) 25–27.
[14] Y. Zhang, J. Xu, B. Lu, J. Alloys Comp. 582 (2014) 635–639.
[15] G.R. Dillip, B.D.P. Raju, J. Alloys Comp. 540 (2012) 67–74.
[16] G.R. Dillip, K. Mallikarjuna, S.J. Dhoble, B.D.P. Raju, J. Phys. Chem. Solids 75 (2014) 8–14.
[17] G.R. Dillip, S.J. Dhoble, B.D.P. Raju, Opt. Mater. 35 (2013) 2261–2266.
[18] L. Wu, Y. Zhang, X.L. Chen, Y.F. Kong, T.Q. Sun, J.J. Xu, Y.P. Xu, J. Solid State Chem. 180 (2007) 1470–1475.
[19] W.B. Im, N.N. Fellows, S.P. DenBaars, R. Seshadri, Y.I. Kim, Chem. Mater. 21 (2009) 2957–2966.
[20] X. Li, L. Guan, M. Sun, H. Liu, Z. Yang, Q. Guo, G. Fu, J. Lumin. 131 (2011) 1022–1025.
[21] A.K. Zak, W.H. Abd Majid, M.E. Abrishami, R. Yousefi, Solid State Sci. 13 (2011) 251–256.
[22] B.S. Ravikumar, H. Nagabhushana, D.V. Sunitha, S.C. Sharma, B.M. Nagabhushana, C. Shivakumara, J. Alloys Comp. 585 (2014) 561–571.
[23] A.I. Borhan, A.R. Iordan, M.N. Palamaru, Mater. Res. Bull. 48 (2013) 2549–2556.
[24] X. Chen, M. Li, X. Chang, H. Zang, W. Xiao, J. Solid State Chem. 180 (2007) 1658–1663.
[25] J. Sun, J. Lai, J. Sun, H. Du, J. Rare Earths 29 (2011) 321–325.
[26] L. Li, W. Zi, G. Li, S. Lan, G. Ji, S. Gan, H. Zou, X. Xu, J. Solid State Chem. 191 (2012) 175–180.
[27] M.R.N. Soares, M.J. Soares, A.J.S. Fernandes, L. Rino, F.M. Costa, T. Monteiro, J. Mater. Chem. 21 (2011) 15262–15265.
[28] X.Y. Sun, J.H. Zhang, X. Zhang, S.Z. Lu, X.J. Wang, J. Lumin. 122 (2007) 955–957.
[29] V.R. Bandi, B.K. Grandhe, H.J. Woo, K. Jang, D.S. Shin, S.S. Yi, J.H. Jeong, J. Alloys Comp. 538 (2012) 85–90.

[30] J. Li, J.G. Li, S. Liu, X. Li, X. Suna, Y. Sakka, J. Mater. Chem. C 1 (2013) 7614–7622.
[31] Q.L. Dai, H.W. Song, M.Y. Wang, X. Bai, B. Dong, R.F. Qin, X.S. Qu, H. Zhang, J. Phys. Chem. C 112 (2008) 19399–19404.
[32] G. Blasse, J. Solid State Chem. 62 (1986) 207–211.
[33] A.K. Parchur, A.I. Prasad, A.A. Ansari, S.B. Rai, R.S. Ningthoujam, Dalton Trans. 41 (2012) 11032–11045.
[34] G. Li, C. Li, C. Zhang, Z. Cheng, Z. Quan, C. Peng, J. Lin, J. Mater. Chem. 19 (2009) 8936–8943.
[35] L. Zhang, H. Zhong, X. Li, L. Cheng, L. Yao, J. Sun, J. Zhang, R. Hua, B. Chen, Phys. B 407 (2012) 68–72.
[36] C.S. McCamy, Color. Res. Appl. 17 (1992) 142–144.